Induction Motor Vector Control Drive with Enhancement Fractional-Order Sliding Mode Based on Rotor Flux Estimation

Mustafa Dursun (mustafadursun@duzce.edu.tr)
Duzce University: Duzce Universitesi https://orcid.org/0000-0001-9952-9358

Research Article

Keywords: Vector control, PI controller, Sliding mode controller, Fractional-order sliding mode controller, MATLAB/Simulink

Posted Date: May 13th, 2022

DOI: https://doi.org/10.21203/rs.3.rs-1438576/v1

Induction Motor Vector Control Drive with Enhancement Fractional-Order Sliding Mode Based on Rotor Flux Estimation

Mustafa DURSUN

Electrical Electronics Engineering Department, Faculty of Engineering, Duzce University, 81620 Konuralp, Duzce/Turkey

e-mail: mustafadursun@duzce.edu.tr

orcid number: 0000-0001-9952-9358

Abstract

In many areas where variable frequency drive is needed, induction motors (IM) play an important role. It is therefore very important to properly control the speed using an induction motor. Three-phase asynchronous motors, especially squirrel-cage asynchronous motors, exhibit non-linear behavior in sudden changes and parameter changes in load and variable speed applications. Therefore, an advanced controller is needed to increase the asynchronous motor performance. This study, it is aimed to develop a Fractional Order Sliding Mode Control (FOSMC) rotor flux and speed controller-based system for a vector-controlled induction motor. The relevant models in this study are made using MATLAB/Simulink software tools. Thus, the performance analysis of the IM, sudden load change, variable reference speed conditions, and motor parameter changes are carried out with the developed controller, and the results were interpreted in detail. It has been seen that the intended method is quite durable under different operating conditions such as sudden load, reverse speed step response, reverse speed sine response, parameter change, compared to classical sliding mode (SM) and proportional-integral (PI) controller designs.

Keywords: Vector control, PI controller, Sliding mode controller, Fractional-order sliding mode controller, MATLAB/Simulink.

INTRODUCTION

Electric motor drives are constantly used in many applications where electrical energy is converted into mechanical energy. They have become an indispensable component in three-phase asynchronous motors, especially due to their well-known advantages such as simple, robust, and low-cost structure. The drivers have made rapid progress thanks to the recent development of microcontrollers and DSPs. The drive controls often become more accurate by sensing three-phase currents and voltages. Therefore, an advanced driver and control structure is needed to increase the performance of asynchronous motors. Many researchers focusing on reducing the implementation cost and creating robust structures to develop control structures have mainly focused on scalar control (SC), direct torque control (DTC), and field-oriented control (FOC) structures [1]. In the last two decades, the vectorial control technique has been the most common method used in asynchronous motor control applications [2,3]. In this method, PI controllers are generally used as speed, torque, and current controllers. These controllers are the most popular controllers used in automated systems due to their robustness, adaptability to system behavior, and convergence to the optimum [3]. These advantages are

only valid in linearity situations as they offer poor robustness in nonlinear systems. Therefore, there is a need for a well-designed nonlinear controller to improve the robustness of nonlinear systems with PID. The most common of these are adaptive control, backstepping control, predictive control, and sliding mode control techniques [4-9]. Among them, the SMC technique has become a more preferred nonlinear control method due to its robust structure, fast response, and good dynamic response on the induction motor [10].

The main disadvantage is the high-frequency chatter problem due to the discontinuous nature of the SMC. This behavior creates wear and tear on mechanical parts and vibration problems in machines. This disadvantage is undesirable during implementation [11-12]. A lot of research has been done to eliminate these negativities. Sigmoid or hyperbolic tangent methods combined with a low-pass filter have been tried, but have generally been found to cause phase shift and low accuracy in the system [13-16]. In addition to the classical SMC controllers, smart controllers such as fuzzy logic controllers (FLC) have also been reported and several hybrid controllers based on the SMC-FLC method for nonlinear systems have been mentioned in the literature [17-19]. The suitable solution to minimize chatter in SMC controllers is to combine FLC controllers with SMC controllers and adjust the discontinuous control gain with FLC. However, it requires intensive mathematical processing and has difficulties in determining membership functions [20-24]. The literature discussed so far has focused on integer-order controllers. In later studies, fractional sliding mode control (FOSMC) started to take place in studies in the literature because it showed superior control performance compared to a proportional and integral controller (PI) and classical sliding mode controller (SMC) [25]. Recently, examples of fractional (non-integer) computation are seen in many interesting fields such as aerospace systems, applied physics, and photovoltaic power generation systems [26-29]. However, a study on the use of FOSMC structure in asynchronous motor drive systems is very few and not detailed in the literature. This control method aims to control the speed and torque of the asynchronous motor against variable structure systems, to reduce the amount of peak value overshoot, to reduce the chatter existing in the conventional sliding mode controller, and to bring the settling time to the desired values by eliminating parameter uncertainties. Therefore, we propose to present a robust FOSMC scheme using the fractional math method in this study. The main contributions of this research are highlighted as follows:

1- The motor is modeled by subtracting the nonlinear dynamic model equations of the IM. Then the asynchronous motor is conventionally controlled by the vector control technique. In this traditional structure, PI controllers are used for speed, torque, and flux.

2- To improve the dynamic performance of the motor, instead of these PI controllers, only the conventional sliding mode control structure is used for rotor flux and speed controllers.

3- Finally, a fractional-order sliding mode controller is used to show superior control performance and a more robust behavior against disruptive effects compared to the classical sliding mode controller. The parameters of the proposed SMC system are adjusted according to the Lyapunov method to ensure the stability of the system.

4- In addition, the DC link voltage is detected in the model to estimate the rotor flux, and three-phase voltages are calculated by using it together with the switching signals, which reduces the need for voltage sensors.

The article is organized as follows: In Chapter 2 the mathematical model of the induction motor is obtained and the field-oriented control method with conventional PI controllers is given, in Chapter 3 the traditional SMC structure is mentioned and its equations are given, in Chapter 4 mathematical equations representing the FOSMC system are extracted and the control structure has been created, the simulation results of these three controllers are shown in Chapter 5, and finally, the results are presented in Chapter 6.

Induction Motor Model Description and Control Design

The direct rotor flux-based vector structure of induction motor control is given in Figure 1. In this control technique, rotor flux estimation is very important as it consists of measurable quantities and the calculation of unmeasurable quantities from the machine model. Since the machine parameters used in the rotor flux estimation block are variable, many observer structures have been proposed in this respect. In this block, the model of the machine in the alpha-beta axis is used. To apply this model, the current and voltage values in the a-b-c axis of the machine must be converted to the alpha-beta axis. In the estimation block, the torque value along with the amplitude and phase of the flux is calculated to be used in torque and flux control. Thus, a control system is created that controls the speed and torque of the machine [1-4]. The model of the three-phase IM can be expressed in the fixed reference frame (alpha-beta) as follows;

$$\dot{x} = Ax + Bu$$
$$y = Cx \tag{1}$$

Here, the induction motor model is given in the state-space form. They are 4x4 and 4x2 sized state matrices containing the motor model equations A and B. C is the unit matrix, y is the output vector, and u and x are the input and state vectors of size 2x1 and 4x1.

$$x = \begin{bmatrix} i_{\alpha s} \\ i_{\beta s} \\ \lambda_{\alpha r} \\ \lambda_{\beta r} \end{bmatrix} \text{ve } u = \begin{bmatrix} u_{\alpha s} \\ u_{\beta s} \end{bmatrix}, y = \begin{bmatrix} i_{\alpha s} \\ i_{\beta s} \end{bmatrix}, C = \begin{bmatrix} 1 & 0 & 0 & 0 \\ 0 & 1 & 0 & 0 \end{bmatrix}$$

$$A = \begin{bmatrix} -\frac{1}{\sigma L_s}\left(R_s + \frac{R_r L_m^2}{L_r^2}\right) & 0 & \frac{L_m R_r}{\sigma L_s L_r^2} & \frac{L_m}{\sigma L_s L_r} p\omega_r \\ 0 & -\frac{1}{\sigma L_s}\left(R_s + \frac{R_r L_m^2}{L_r^2}\right) & -\frac{L_m}{\sigma L_s L_r} p\omega_r & \frac{L_m R_r}{\sigma L_s L_r^2} \\ \frac{L_m R_r}{L_r} & 0 & -\frac{R_r}{L_r} & -p\omega_r \\ 0 & \frac{L_m R_r}{L_r} & p\omega_r & -\frac{R_r}{L_r} \end{bmatrix}$$

$$B = \begin{bmatrix} \frac{1}{\sigma L_s} & 0 \\ 0 & \frac{1}{\sigma L_s} \\ 0 & 0 \\ 0 & 0 \end{bmatrix}$$

$$\frac{d\omega_r}{dt} = -\frac{B}{J}\omega_r + \frac{1}{J}(T_e - T_L) \tag{2}$$

$$T_e = \frac{3}{2} p \frac{L_m}{L_r}\left(\lambda_{\alpha r} i_{\beta s} - \lambda_{\beta r} i_{\alpha s}\right) = K_T\left(\lambda_{\alpha r} i_{\beta s} - \lambda_{\beta r} i_{\alpha s}\right) \tag{3}$$

Here, $K_T = (3/2)\, p\, (L_m/L_r)$ ve $\sigma = 1 - (L_m^2/L_s L_r)$.

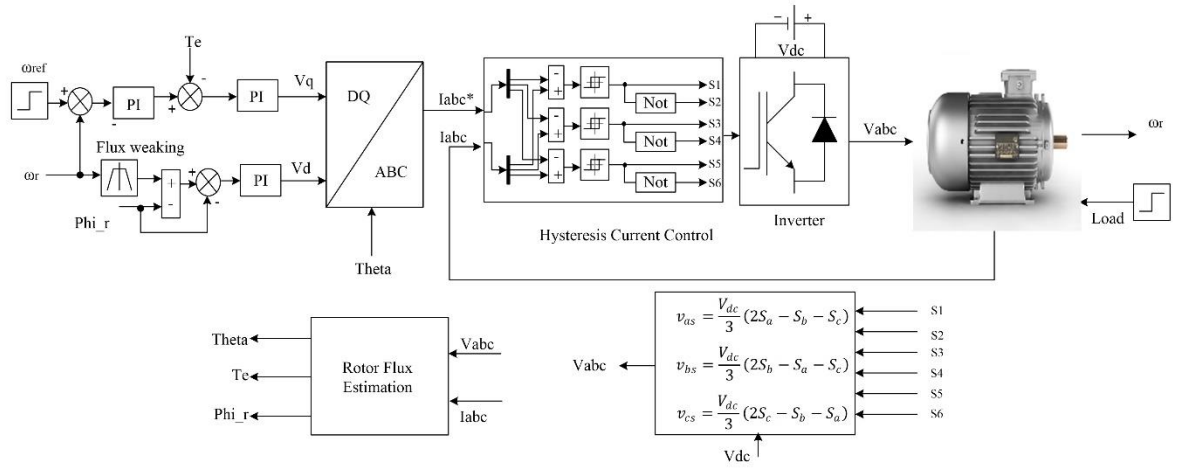

Figure 1. Asynchronous motor rotor flux based vector control design

The hysteresis PWM method is preferred in the system so that the switching elements used in the inverter respond quickly and maintain the desired current waveform. The control loop for switching is:

$i_{as} < (i_{as}^* - h) \rightarrow S_1\ on\ S_4\ off$

$i_{as} < (i_{as}^* - h) \rightarrow S_1\ off\ S_4\ on$

$i_{bs} < (i_{bs}^* - h) \rightarrow S_3\ on\ S_6\ off$

$i_{bs} < (i_{bs}^* - h) \rightarrow S_3\ off\ S_6\ on$

$i_{cs} < (i_{cs}^* - h) \rightarrow S_5\ on\ S_2\ off$

$i_{cs} < (i_{cs}^* - h) \rightarrow S_5\ off\ S_2\ on$

Here $(i_{as}^*, i_{bs}^*, i_{cs}^*)$ are the reference currents generated by the vector control method. (S1, S3, S5) are the upper switches of the inverter and (S2, S4, S6) are the lower switches. The ideal

phase voltage outputs of the inverter can be calculated from the DC bus input of the inverter and the basic gate pulses as follows:

$$v_{as} = \frac{V_{dc}}{3}(2S_a - S_b - S_c) \tag{4}$$

$$v_{bs} = \frac{V_{dc}}{3}(2S_b - S_a - S_c) \tag{5}$$

$$v_{cs} = \frac{V_{dc}}{3}(2S_c - S_b - S_a) \tag{6}$$

In this structure, the three-phase AC voltage estimation method is used with the measurement taken from the switching signals and DC bus voltage. In this way, there is no need for extra voltage sensors in the motor circuit and the drive system has become more economical.

Flux Estimation Model

The stator flux vector is obtained by taking the difference of the voltage falling on the stator resistance from the stator voltage [4].

$$\lambda_s = \int (v_s - i_s R_s) \tag{7}$$

Thus, according to the alpha-beta stator flux relation, the flux equation in the alpha-beta plane is obtained as follows;

$$\lambda_{\alpha s} = \int (v_{\alpha s} - i_{\alpha s} R_s) \tag{8}$$

$$\lambda_{\beta s} = \int \left(v_{\beta s} - i_{\beta s} R_s\right) \tag{9}$$

From the induction motor model, the stator and rotor fluxes in the α-β plane are calculated as follows;

$$\lambda_{\alpha s} = i_{\alpha s} L_s + i_{\alpha r} L_m \tag{10}$$

$$\lambda_{\beta s} = i_{\beta s} L_s + i_{\beta r} L_m \tag{11}$$

$$\lambda_{\alpha r} = i_{\alpha r} L_r + i_{\alpha s} L_m \tag{12}$$

$$\lambda_{\beta r} = i_{\beta r} L_r + i_{\beta s} L_m \tag{13}$$

If we rearrange the equations, we get the α-β components of the rotor currents as follows.

$$i_{\alpha r} = \frac{1}{L_m}(\lambda_{\alpha s} - i_{\alpha s} L_s) \tag{14}$$

$$i_{\beta r} = \frac{1}{L_m}\left(\lambda_{\beta s} - i_{\beta s} L_s\right) \tag{15}$$

It is obtained in the form. The resultant rotor flux amplitude and phase angle from the rotor flux components are also calculated below.

$$\lambda_r = \sqrt{\lambda_{\alpha r}^2 + \lambda_{\beta r}^2} \tag{16}$$

$$\theta = tan^{-1}\frac{\lambda_{\beta r}}{\lambda_{\alpha r}} \tag{17}$$

Figure 2 shows the block diagram of the flux estimation algorithm consisting of these equations.

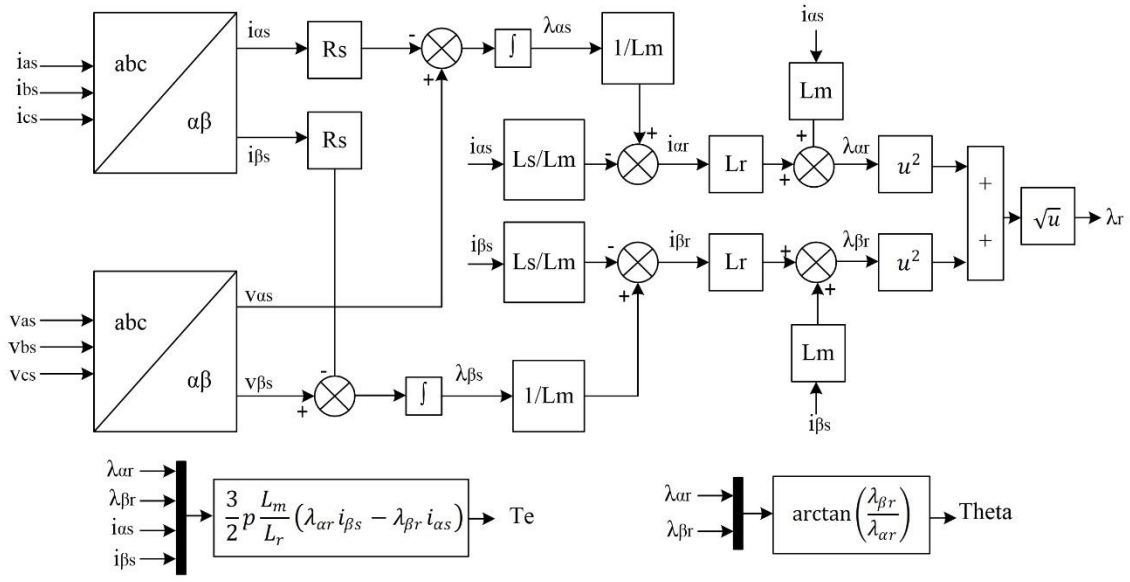

Figure 2. Rotor flux estimation block

Sliding Mode Control

The sliding mode speed and flux controllers must track the system state variable along the sliding surface. In the FOC technique, the mechanical equation of the machine is defined as in (18);

$$T_e = K_T i_{qs} \tag{18}$$

Here K_T is the moment constant and is defined as follows;

$$K_T = \frac{3}{2} p \frac{L_m}{L_r}(\lambda_{dr}) \tag{19}$$

Mechanical equation of induction motor;

$$T_e = J\dot{\omega}_m + B\omega_m + T_L \tag{20}$$

If the expression $K_T i_{qs}$ is written instead of Te;

$$bi_{qs} = \dot{\omega}_m + a\omega_m + f \tag{21}$$

Here $a = B/J, b = K_T/J \; ve \; f = T_L/J$. This equation is represented in Equation (22) with the uncertainties Δa, Δb, and Δf in the terms a, b, and f:

$$\dot{\omega}_m = -(a + \Delta a)\omega_m - (f + \Delta f) + (b + \Delta b)i_{qs} \tag{22}$$

The tracking speed error is defined as:

$$e(t) = \omega_m^*(t) - \omega_m(t) \tag{23}$$

Here ω_m^* is the rotor speed reference. If we take the derivative of Equation (23);

$$\dot{e}(t) = \dot{\omega}_m^*(t) - \dot{\omega}_m(t) = -ae(t) + u(t) + d(t) \tag{24}$$

Here:

$$u(t) = bi_{qs} - a\omega_m^*(t) - f(t) - \dot{\omega}_m^*(t) \tag{25}$$

and d(t) uncertainty;

$$d(t) = -\Delta a\omega_m^*(t) - \Delta f(t) + \Delta bi_{qs} \tag{26}$$

The traditional sliding mode structure is one of the first used control algorithms and uses a sliding surface as given in Equation (27):

$$s = \left(\frac{d}{dt} + \lambda\right)e \tag{27}$$

Here λ is a positive constant and is called the bandwidth. This constant, which also concerns controller performance, is closely related to system performance. When there is a derivative component on the sliding surface, it causes a steady-state error in the system [10]. In addition, conventional shift mode controllers are also affected by noise because they use the derivative of the error [11]. For this reason, it is necessary to pass the error through a low-pass filter. At this point, it has come to mind that PI controllers act as low-pass filters. In that case, if a slip surface structure using an integrator is installed instead of the derivative component, we will not only avoid using a low pass filter but also a controller that is less affected by noise will be obtained. Also, with the use of an integrator, we can get rid of the steady-state error, which is important in control. For this reason, the slip surface is defined as in Equation (28):

$$s_1(t) = e(t) - \int_0^t (k - a)e(\tau) \tag{28}$$

Here k; is the gain constant and following the reference, speed is based on the assumption [28]:

1- The gain constant k should be chosen such that; Let the value (k-a) be negative. For this, it is sufficient to choose k<0. It was said that s (t) = 0 when the slip surface is reached. The control rule that must be applied to remain on the sliding surface is defined as follows:

$$u(t) = ke(t) - \beta sgn(s_1) \tag{29}$$

$$sgn(s_1) = \begin{cases} 1 & if\ s_1 > 0 \\ 0 & if\ s_1 = 0 \\ -1 & if\ s_1 < 0 \end{cases}$$

β, which is the coefficient of the signum switching function; is called the switching gain. Another assumption for the selection of this gain should be as follows:

2- The switching gain β should be chosen such that it must be greater than or equal to the absolute value of the sum of the uncertainties in all operating conditions. Well;

$\beta \geq |\, d\,(t)\,|$

The drive control system needs to be stable. Therefore, it is necessary to approach the operating point. If these two assumptions are met, the control rule given by (29) takes the speed tracking error to zero as time goes to infinity. The proof of this is provided by the Lyapunov stability analysis. Let the Lyapunov function be defined as:

$$V(t) = \frac{{s_1}^2(t)}{2} \tag{30}$$

Taking the derivative of this function becomes:

$$\dot{V}(t) = s_1(t)\dot{s_1}(t) \tag{31}$$

When equation (28) is substituted in (31):

$$\dot{V}(t) = s_1[\dot{e} - (k - a)e] \tag{32}$$

By making use of equation (24), equation (33) takes the form:

$$\dot{V}(t) = s_1[(-ae + u + d) - (ke - ae)] = s_1[u + d - ke] \tag{33}$$

Combining Equation (33) with (29), using assumption #2:

$$\dot{V}(t) = s_1[ke - \beta sgn(s_1) + d - ke] = s_1[d - \beta sgn(s_1] \leq |\beta - |d||s_1| \leq 0 \tag{34}$$

It is also used here in the definition:

$$s_1(t) = |s_1(t)|sgn(s_1(t)) \tag{35}$$

Thus, using the Lyapunov stability theorem, the following rules, which are necessary for the sliding mode method, are obtained:

a- The positivity of V(t) is assured by the appropriate function selection.
b- The negativity of $\dot{V}(t)$ is assured.
c- $S_1(t)$ goes to infinity while V(t) goes to infinity. At $S_1(t) = 0$ the system is asymptotically stable. Also, all the orbits of the system are forced to be $S_1(t) = 0$ in a finite time and remain on this surface after reaching the slip surface.

The physical meaning of $S_1(t) = 0$ for the system means that the system is seated on the slip surface. So $\dot{s}(t)$ is equal to zero. The dynamic behavior of the tracking problem in equation (24) is checked by Equation (36):

$$\dot{s_1}(t) = 0 \rightarrow \dot{e}(t) = (k - a)e(t) \tag{36}$$

As can be seen from Equation (36), the error function e(t) converges to zero exponentially with assumption number 1. Thus, using equations (24) and (29) together, the control input v_1 should be that:

$$v_1 = \frac{1}{b}[ke - \beta sgn(s_1) + a\omega_m^* + \dot{\omega}_m^* + f] \tag{37}$$

It is obtained as, on the other hand, a sliding mode flux controller is designed to track system variables across the sliding surface.

$$e_2(t) = \lambda_r^* - \lambda_r \tag{38}$$

Taking the derivative of the equation:

$$\dot{e}_2(t) = \dot{\lambda}_r^* - \dot{\lambda}_r \tag{39}$$

The induction motor flux equation is as in Equation (40).

$$\frac{d\lambda_r}{dt} = -\frac{R_r}{L_r}\lambda_r + \frac{L_m R_r}{L_r \lambda_r}\left(i_{\alpha s}\lambda_{\alpha r} + i_{\beta s}\lambda_{\beta r}\right) \tag{40}$$

In this equation, if the derivative value of the flux is substituted in Equation (39).

$$\dot{e}_2(t) = \frac{R_r}{L_r}\lambda_r - \frac{L_m R_r}{L_r \lambda_r}\left(i_{\alpha s}\lambda_{\alpha r} + i_{\beta s}\lambda_{\beta r}\right) + \dot{\lambda}_r^* \tag{41}$$

It is obtained. The slip surface to s_2 for rotor flux can be defined as:

$$s_2 = e_2(t) + C_1 \int e_2 dt \tag{42}$$

Here C_1 is the time constant of the slip surface. Derivative of the sliding surface (S_2):

$$\dot{s}_2 = \dot{e}_2(t) + C_1 e_2(t) \tag{43}$$

Substituting the value of $\dot{e}_2(t)$ from Equation (41) in Equation (43) we get Equations (44) and (45):

$$\dot{s}_2(t) = \frac{R_r}{L_r}\lambda_r - \frac{L_m R_r}{L_r \lambda_r}\left(i_{\alpha s}\lambda_{\alpha r} + i_{\beta s}\lambda_{\beta r}\right) + \dot{\lambda}_r^* + C_1 e_2(t) \tag{44}$$

$$\dot{s}_2(t) = x - y + \dot{\lambda}_r^* + Ce_2(t) \tag{45}$$

'y', a function of rotor flux, depends on rotor resistance and inductance.

$$y = \frac{L_m R_r}{L_r \lambda_r}\left(i_{\alpha s}\lambda_{\alpha r} + i_{\beta s}\lambda_{\beta r}\right) = D\left(i_{\alpha s}\lambda_{\alpha r} + i_{\beta s}\lambda_{\beta r}\right) \quad (46)$$

$$x = \frac{R_r}{L_r}\lambda_r = Z\lambda_r \quad (47)$$

$$Z = \frac{R_r}{L_r} \quad (48)$$

$$D = \frac{L_m R_r}{L_r \lambda_r} \quad (49)$$

Here, the variables Z and D are time-dependent or state-dependent control gains, but the limits are determined as follows:

$$Z_{min} \le Z \le Z_{max}$$

$$D_{min} \le Z \le D_{max}$$

Continuous control law can be formed by providing the $\dot{s}_2 = 0$ slip state from Equation (45). These defined control laws shown in Figure 3b can be interpreted as in Equation (50):

$$\tilde{y} = \tilde{x} + \dot{\lambda}_r^* + Ce_2(t) \quad (50)$$

Here,

$$\tilde{x} = \tilde{Z}\lambda_r$$

$$\tilde{y} = \tilde{D}\left(i_{\alpha s}\lambda_{\alpha r} + i_{\beta s}\lambda_{\beta r}\right) \quad (51)$$

(1/2)(d/dt) (s_2) ≤ η|s| Regardless of the uncertainties on the dynamics, according to the slip condition rule, the discontinuity is added to the term $\tilde{y}_1$ along with the slip surface $\dot{s} = 0$, from which the form Equation (50) is obtained:

$$v_2 = \tilde{D}^{-1}\left\{\tilde{x} + \dot{\lambda}_r^* + Ce_2(t) - Wsgn(s_2)\right\} \quad (52)$$

Here C is the gain constant and its value is (k-a). (W) is the control discontinuity gain. Its value is very important to ensure stability across the surface. The (W) value may change due to uncertainties in the parameters. Sgn is a sign function that can be interpreted as:

$$sgn(s_2) = +1 \; if \; s_2 > 0 \text{ ve } sgn(s_2) = -1 \; if \; s_2 < 0$$

To ensure the stability of the system, the conditions in Equation (53) are obtained similarly for the slip surface S_2:

$$Wsgn(s_2) \ge -\tilde{x} + \tilde{D} - \left(\tilde{D}D^{-1} - 1\right)\left(\dot{\lambda}_r^* + Ce_2(t)\right) + \tilde{D}D^{-1}\eta_2 \quad (53)$$

Therefore, W value, which is the control discontinuity gain that will ensure the stability of the system, can be obtained from Equation (53), and if the value of this gain is high enough, SM will form on the surface of $S_2 = 0$ [30-32].

In all the operations, it is seen that the sliding mode controllers can operate insensitively despite the uncertainties of the system and disturbing inputs. In terms of performance, it will be compared with the PI controller. The blocks created in MATLAB-Simulink are given in Figures 3a and b.

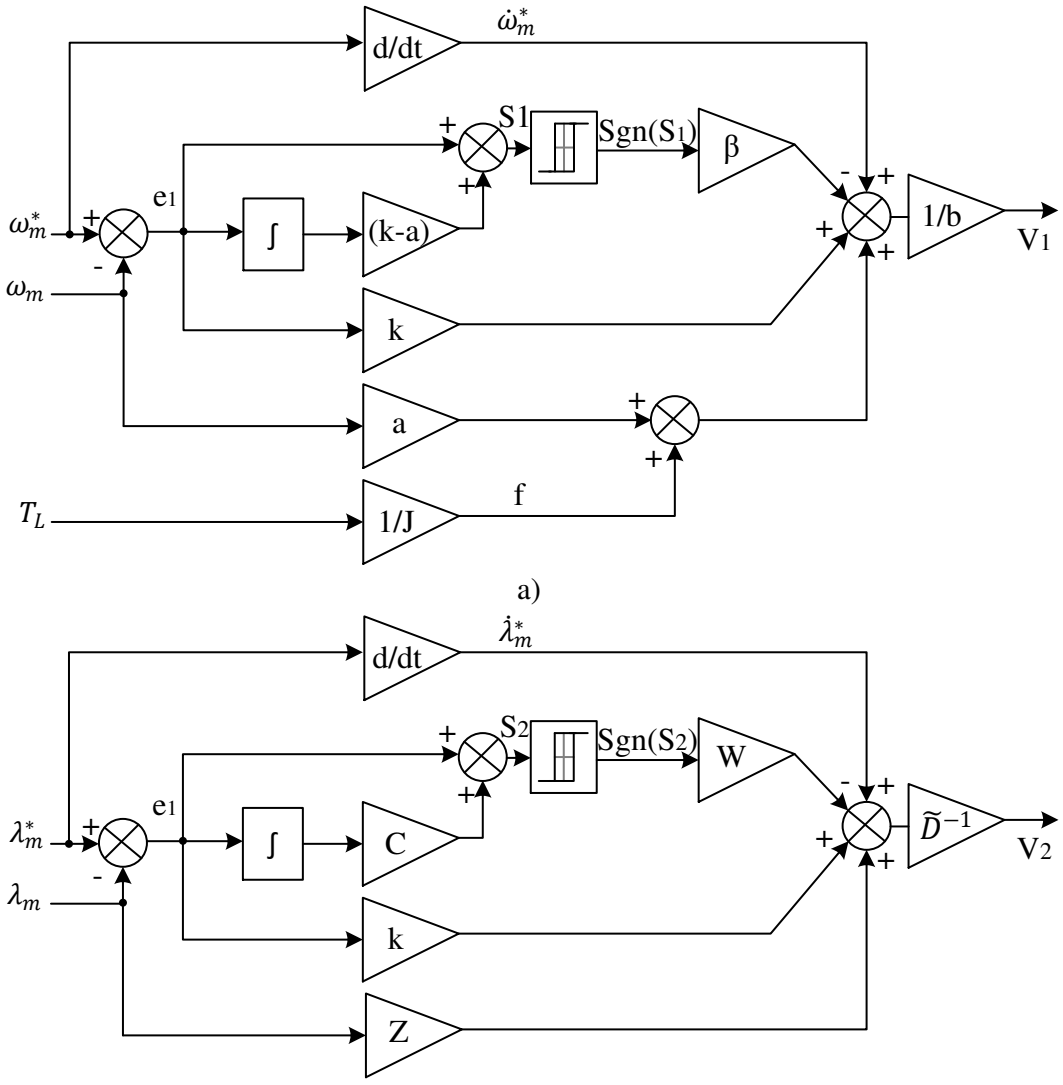

Figure 3. Simulink blocks from SMC's equations (a) speed controller and (b) flux controller

Fractional Order Calculus

Fractional calculus is a solution technique that has been known since the development of integer order (IO) calculus [25-26]. However, for a long time, it has only been accepted as a solution to mathematical problems. In recent years, fractional degree models and controls have been successfully used in many experimental platforms such as system analysis, DC motor speed control, heat flow, and plasma position control [27-28,33]. In all these experiments, compared to IO controllers, FO controllers can better cope with noise and distortion effects and can also significantly reduce the required control function. Due to such superior advantages of fractional order, in this study, the sliding mode control was redesigned on this calculation and used as an

asynchronous motor controller. The most basic expression of the fraction operator is denoted by a general base operator ${}_aD_t^r$ as a generalization of the derivative and integral operators defined as follows. Here r is the gain of the sliding surface and ${}_aD_t^r$ is the fractional operator.

$$D^r \triangleq {}_aD_t^r = \begin{cases} \dfrac{d^r}{dt^r} & R(r) > 0 \\ 1 & R(r) = 0 \\ \displaystyle\int_a^t (d\tau)^{-r} & R(r) < 0 \end{cases}$$

Here the bounds of the operations a and t, the degree of operations r, and in general r ϵ R and r can be a complex number. There are three most commonly used definitions for the mathematical realization of general fractional integro-differential equations. The Riemann–Liouville (RL) definition, the Caputo definition, and the Grunwald–Letnikov (GL) definition [34-36]. The definition of Grunwald-Letnikov (GL) is given as follows;

$${}_aD_t^\lambda f(t) = lim_{h\to 0}(h)^{-\lambda} \sum_{j=0}^{\left[\frac{t-a}{h}\right]} (-1)^j \binom{\lambda}{j} f(t-jh) \tag{54}$$

The Caputo definition of a continuous function is as in the following equation;

$$\alpha D_x^\lambda f(t) = \frac{1}{\Gamma(\lambda-n)} \int_\lambda^t \frac{f^n(\tau)}{(x-\tau)^{\lambda-n+1}} d\tau \tag{55}$$

The λth-order Riemann-Liouville (RL) fractional integration is expressed as;

$${}_aD_t^\lambda f(t) = \frac{1}{\Gamma(\lambda-n)} \int_a^t \frac{f(\tau)}{(x-\tau)^{\lambda-n+1}} d\tau \tag{56}$$

Here should be n-1 < λ < n. Again, the expression Γ(.) is known as the Gamma function. In the Caputo derivative, the initial conditions of fractional differential equations are in the same form as integer differential equations. In addition to these, it is inevitable to use some special functions in fractional-order systems and calculations.

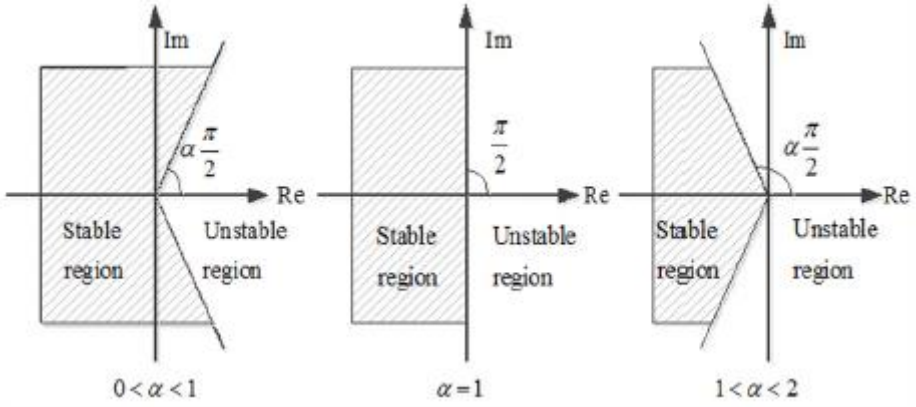

Figure 4. Stable regions for 0<α<2

Figure 4 shows the stable region for 0<α<2. Obviously, the stable region of the fractional system with 0<α<1 is larger than the other two cases [37].

Enhancement of Fractional Order Sliding Mode Control

The block diagram of the designed control system is shown in Figure 5. The purpose of the system is to approximate the angular velocity ω_m to the angular velocity ω_m^* (reference). This means that the tracking error asymptotically approaches zero for any random initial condition and uncertainty. It is well known that the most important point of the SMC method is the formation of (t),s(t)ϵR slip surfaces, and the fulfillment of the control law. As explained earlier, the equations obtained from the speed control equations of classical sliding mode control are as in Equation (57).

$$\begin{aligned} u(t) &= bi_{qs} - a\omega_m^*(t) - f(t) - \dot{\omega}_m^*(t) \\ d(t) &= -\Delta a\omega_m^*(t) - \Delta f(t) + \Delta bi_{qs} \\ \dot{e}(t) &= -ae(t) + u(t) + d(t) \end{aligned} \tag{57}$$

By making use of these equations, the fractional sliding surface is designed as in Equation (58);

$$s = ce(t) + {}_0D_t^r e(t) \tag{58}$$

Here c is a positive gain value and ${}_0D_t^r(.)$ is a fractional degree integral (0 < r < 1). According to the sliding mode control law;

$$\dot{s} = -\gamma s - \xi sign(s) \tag{59}$$

Here γ, ξ ϵ R^+, sign(.) is the defined signum function as in conventional sliding mode. In ideal conditions (d(t)=0), we obtain the derivative of the control surface from the equations (57) and (58) as in Equation (60);

$$\dot{s} = \frac{ds}{dt} = \frac{d}{dt}\left({}_0D_t^r e(t) + ce(t)\right) = {}_0D_t^{r+1} e(t) + c(-ae(t) + u(t) + d(t)) \tag{60}$$

We can obtain the control output from Equations (59) and (60) as in Equation (61);

$$\begin{aligned} i_{qs} = (bc)^{-1}\big[{}_0D_t^{r+1} e(t) - c\big(f(t) + a\omega_m^*(t) + \dot{\omega}_m^*(t) - \gamma e(t)\big) + \gamma\, {}_0D_t^r e(t) \\ + \xi sign(s)\big] \end{aligned} \tag{61}$$

According to these calculations, the block diagram of the proposed controller is shown in figure 5.

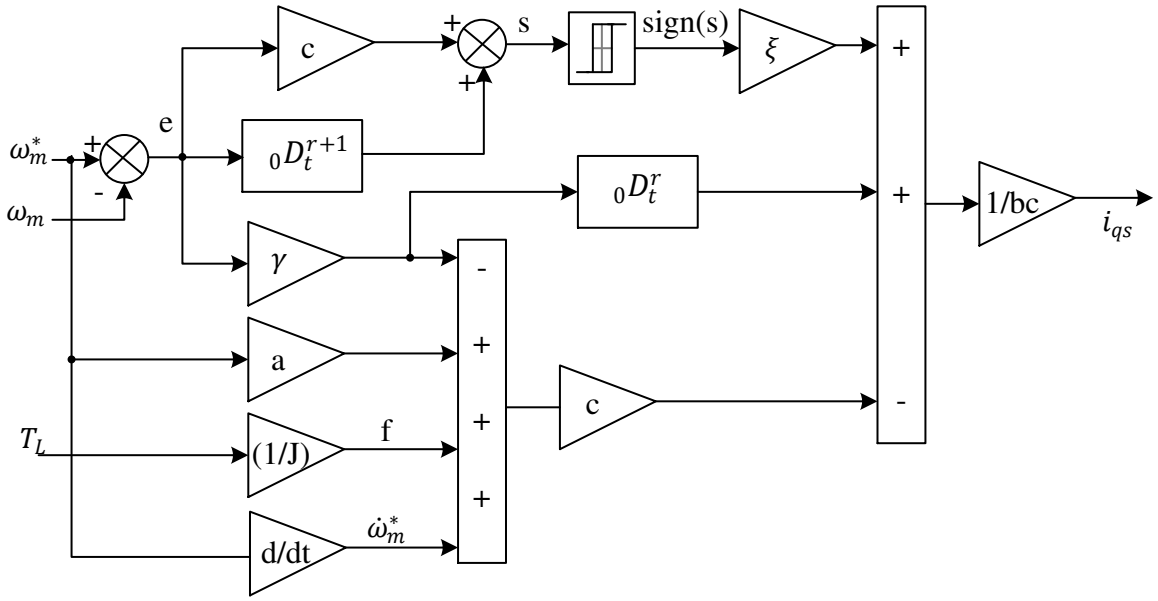

Figure 5. Designed FOSMC block diagram

Stability Analysis

For FOSMC, the stability analysis should satisfy both the achievement condition of the proposed fractional switching manifold and the stability of the fractional-order system. Therefore, the stability analysis has been studied in two steps.

Step 1: It should prove that the proposed fractional-order switching manifold satisfies the reaching condition. This means that the initial state, the control output, can maintain convergence of the initial state to the sliding manifold.

Suppose the system initial states (t0)≠a0, the Lyapunov function candidate is selected as follows:

$$V = \frac{1}{2}s^2 \tag{62}$$

Taking the derivative of V concerning time,

$$\dot{V} = s \times \dot{s} \tag{63}$$

If equations (57), (59), and (60) are substituted in (63),

$$\begin{aligned} \dot{V} = s \times \dot{s} &= s \times \frac{d}{dt}[ce(t) + {}_0D_t^r e(t)] \\ &= s \times [{}_0D_t^{r+1} e(t) + c(-ae(t) + u(t) + d(t))] \\ &= s \times (-\xi sign(s) + cd(t) - \gamma s) = -\xi|s| + cd(t)s - \gamma s^2 \end{aligned} \tag{64}$$

It is obtained. Thus, if the following condition is satisfied,

$\xi > c|d(t)| \Rightarrow \xi/c > |d(t)|$

$\dot{V} < 0$ will be valid. Assuming $|d(t)| \leq u \, \epsilon \, R^+$ from here, according to the Lyapunov stability theorem, if $\xi/c > u$, the condition that the sliding mode controller will be satisfied.

Explanation: The control law (1) directs the system to converge to the switching manifold in a finite time.

Proof: If s(t0)>0, the initial state of the switching manifold is satisfied, Equation (59) can be constructed as::

$$\dot{s} = -\gamma s - \xi \tag{65}$$

The solution of Equation (65),

$$s = [s(t_0) + \gamma^{-1}\xi]e^{-\gamma(t-t_0)} - \gamma^{-1}\xi \tag{66}$$

Inappropriate time conditions:

$$t = t_0 - \frac{1}{\gamma} ln \frac{\xi}{\gamma s(t_0) + \xi} \tag{67}$$

The system converges to the switching manifold. Similarly, if the initial state of the switching manifold satisfies s(t0)<0, then under appropriate time conditions:

$$t = t_0 - \frac{1}{\gamma} ln \frac{\xi}{\xi - \gamma s(t_0)} \tag{68}$$

The system again approaches the switching manifold. Therefore, if the following inequality is satisfied, the system converges to the switching manifold at any initial state.

$$t \geq t_0 - \frac{1}{\gamma} ln \frac{\xi}{\gamma |s(t_0)| + \xi} \tag{69}$$

Step 2: To prove that the fractional-order system is stable and converges, the states must come to an equilibrium point quickly and steadily as soon as a slip mode occurs. To prove the stability of the proposed fractional-order slip mode, the following theorem must be satisfied.

Theorem: System (58) is stable and its state (error) decreases from t^{-r} to 0 if the following two conditions are true.

$c > 0$

$0 < r < 1$

Proof: System 58 is rewritten when sliding mode occurs,

$$_0D_t^r e(t) = -ce(t) \tag{70}$$

Thus, c > 0 and 0 < r < 1 are provided simultaneously, the system 58 is stable and its state (error) decreases from t^{-r} to 0.

Simulation Result And Discussions

For simulation studies, 3kW, 415V, 50Hz, 1430 rpm, 4-pole IM is used. In Figure 1, the performance of the IM driver system with the rotor flux-based vector control technique is examined. The traditional SMC algorithm is given in Figure 3 and the FOSMC algorithm developed in Figure 5 is given. All these algorithms are implemented in MATLAB/Simulink environment. To prove the dynamic performance of the proposed FOSMC technique, comparisons are made with PI and SM controllers under different operating conditions. The motor parameters used for the simulation are given in Table 1.

Table 1 Parameters of IM

Nominal Power (W)	3000 W
Voltage (line-line) (V)	220 V
Frequency (Hz)	50 Hz
Stator Resistance, Rs	1.45 ohm
Rotor Resistance, Rr	1.93 ohm
Stator Inductancei Lls	12.2 mH
Rotor Inductance, Llr	2.66 mH
Mutual Inductance, Lm	187.8 mH
Inertia, J	0.008 kg.m^2
Friction factor, Bm	0.003 N.m.s
Pole pairs, p	2

Three different design states such as PI, SMC, and FOSMC are applied to the same induction motor to control the performance of the proposed FOSM controller. First of all, in Figure 6, the motor was examined at low-medium and high speeds without load. It was then tested in the inverse velocity and sine reference velocity conditions in Figure 7 (a) and (b).

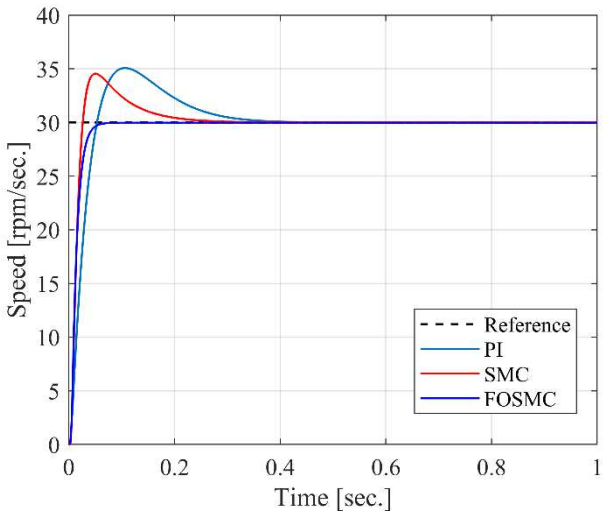

(a)

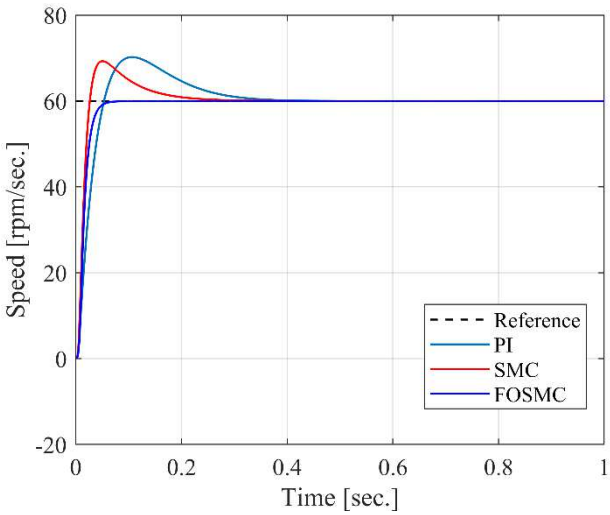

(b)

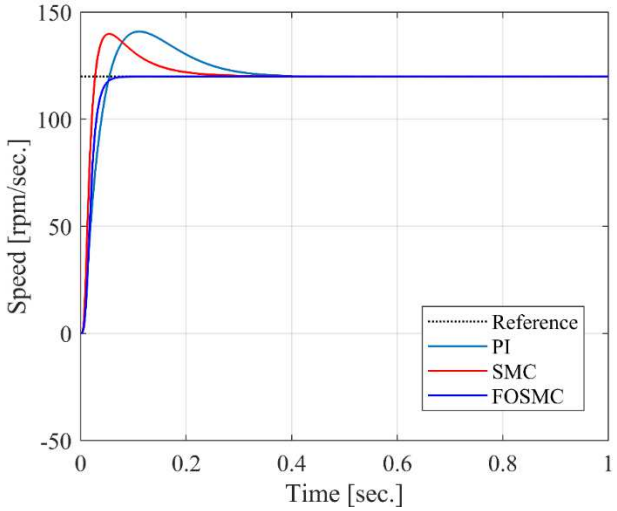

(c)

Figure 6. Responses of Induction Machine with the constant speed with no-load, a)low, b)medium, c) high-speed condition

Figure 6 shows the performance of the machine when the engine is running for 1s with a constant speed reference of 30-60 and 120 rpm/sec. As seen in graphs (a), (b), and (c), the proposed FOSMC structure in low-medium and high-speed situations can track the desired reference speed better than other control structures with zero overshoot and low error in steady-state (less than 1 rpm). Table 2 also includes the values of overshoot and settling times.

Table 2. (TL=0 N.m) Amount of overshoot and settling time of speed

Control method	**Speed (rpm/sec.)**	**Overshoot (rpm)**	**Settling Time (sec)**
PI	30	5	0.4
SMC	30	4	0.3
FOSMC	30	**0**	**0.08**
PI	60	10	0.4
SMC	60	10	0.3
FOSMC	60	**0**	**0.08**
PI	120	20	0.4
SMC	120	20	0.3
FOSMC	120	**0**	**0.08**

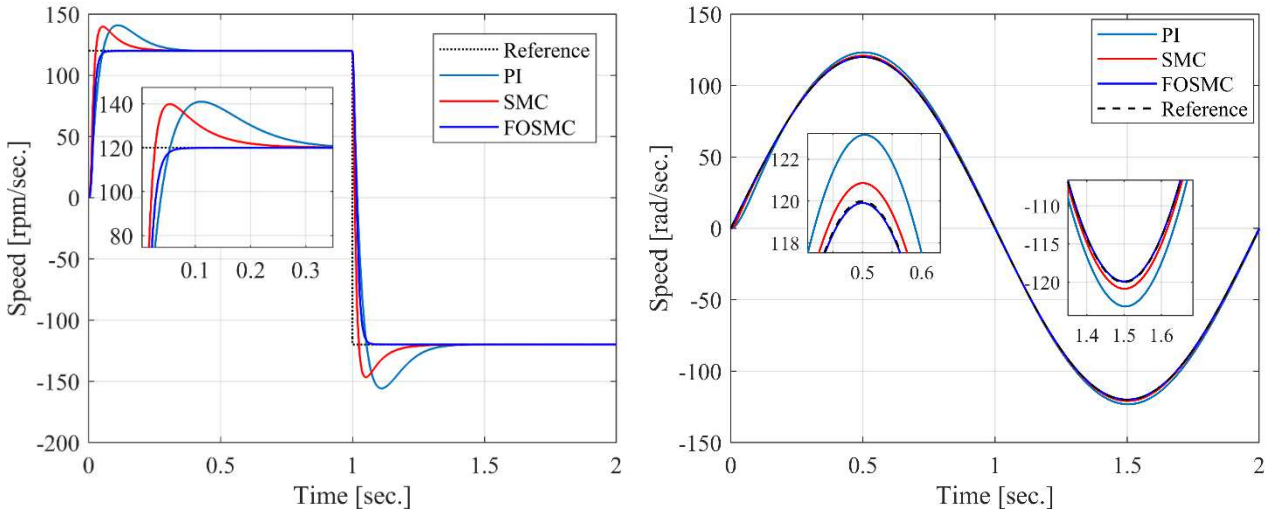

(a) (b)

Figure 7. Speed responses with no-load, a)120 rad/sec. to -120 rad/sec. step response, b) 120 rad/sec. to -120 rad/sec. sinusoidal response

In Figure 7 (a), the speed response of the motor is examined according to the square wave speed reference. Initially, in both cases, the motor is accelerated with no load and in the case of the PI controller, the machine reaches a reference speed of 120 rpm/sec with an overshoot of 20 rpm/sec. in t=0.4 seconds while in the case of the SM controller the machine reaches 120 rpm/sec. with an overshoot of 20 rpm/s. It reaches the reference speed of /s in t=0.3 seconds. However, in the proposed FOSM controller structure, the machine has 0 rpm/sec. overshoot, it reaches a reference speed of 120 rad/s in t=0.08 seconds. In (b), in the case of sine wave speed reference, the proposed controller structure reaches the desired reference more stable than other controller structures. It is also better in terms of setting time, overshoot, steady-state error. The values related to these are also given in Table 3. As can be seen, the best response is obtained in the proposed FOSMC structure in positive and negative speed conditions.

Table 3. (TL=0 N.m) Overshoot and settling time at different reference speeds

Control method	**Speed (rpm/sec.)**	**Overshoot (rpm)**	**Settling Time (sec)**
PI	120 square wave	20	0.4
SMC	120 square wave	20	0.3
FOSMC	120 square wave	**0**	**0.08**
PI	120 sinus wave	3	0.2
SMC	120 sinus wave	1	0.125
FOSMC	120 sinus wave	**0**	**0.08**

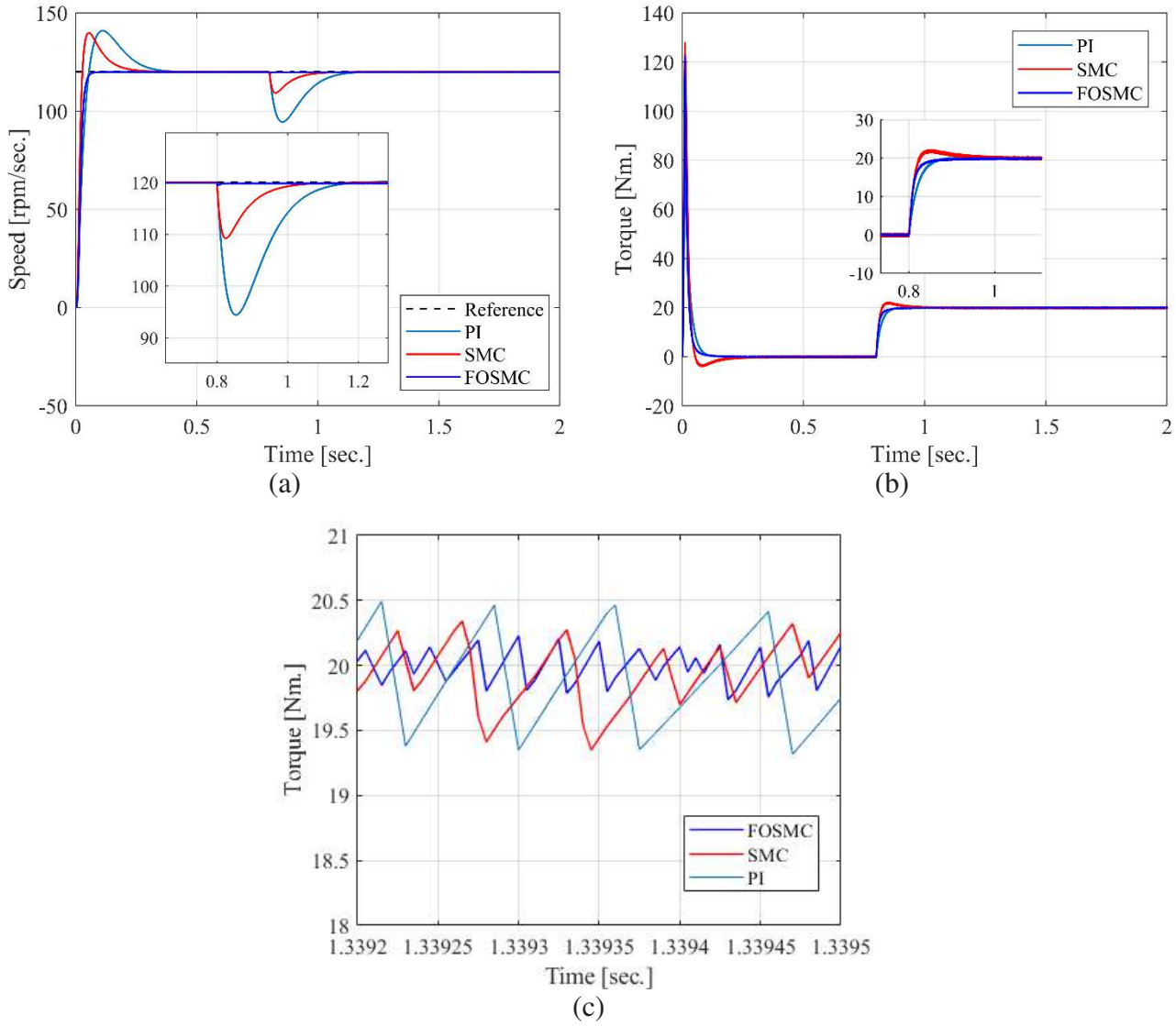

Figure 8. Speed responses with 20Nm-load at 0.8 sec., a)120 rad/sec. speed response, b) Torque response, c) Torque response zoom

In Figure 8(a) is applied 120 rpm/sec. reference speed and a load torque of 20 Nm at 0.8. sec. In the proposed control structure, the speed drops to 198 rpm/sec. as soon as the load is applied, while in other control structures there is a much greater decrease, meaning the recovery time is faster and the response offers less oscillation. However, while the steady-state error goes to zero in other control structures, it remains at 1 rpm in the proposed structure. (b) shows the torque-speed graph. A torque of 20 Nm is applied in 0.8 seconds, and it is the proposed structure that showed the best settling time to the reference speed in a very fast time of 0.85 seconds. Also in the third graph (c), the electromagnetic torque shows a smoother and therefore less chatter.

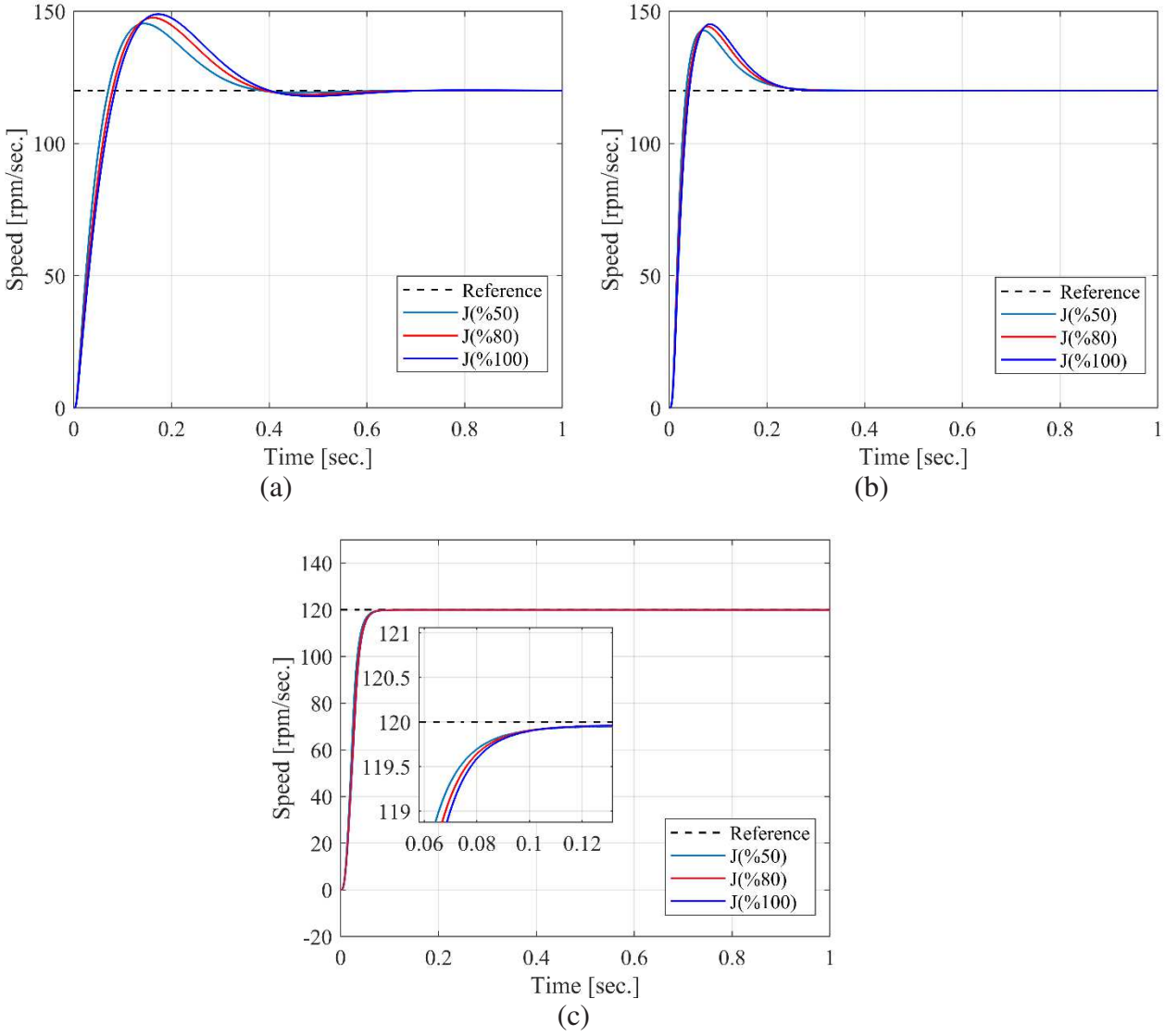

Figure 9. Speed responses variation of J parameter a) Conventional PI control b) SMC control, c) FOSM control

In Figure 9, the response of the motor to the moment of inertia changes is examined. As can be seen, the proposed FOSMC structure shows the best response at 50-80% and 100% increases in the moment of inertia. While the durations such as overshoot and settling time increased in other control structures, the proposed control structure was almost unaffected.

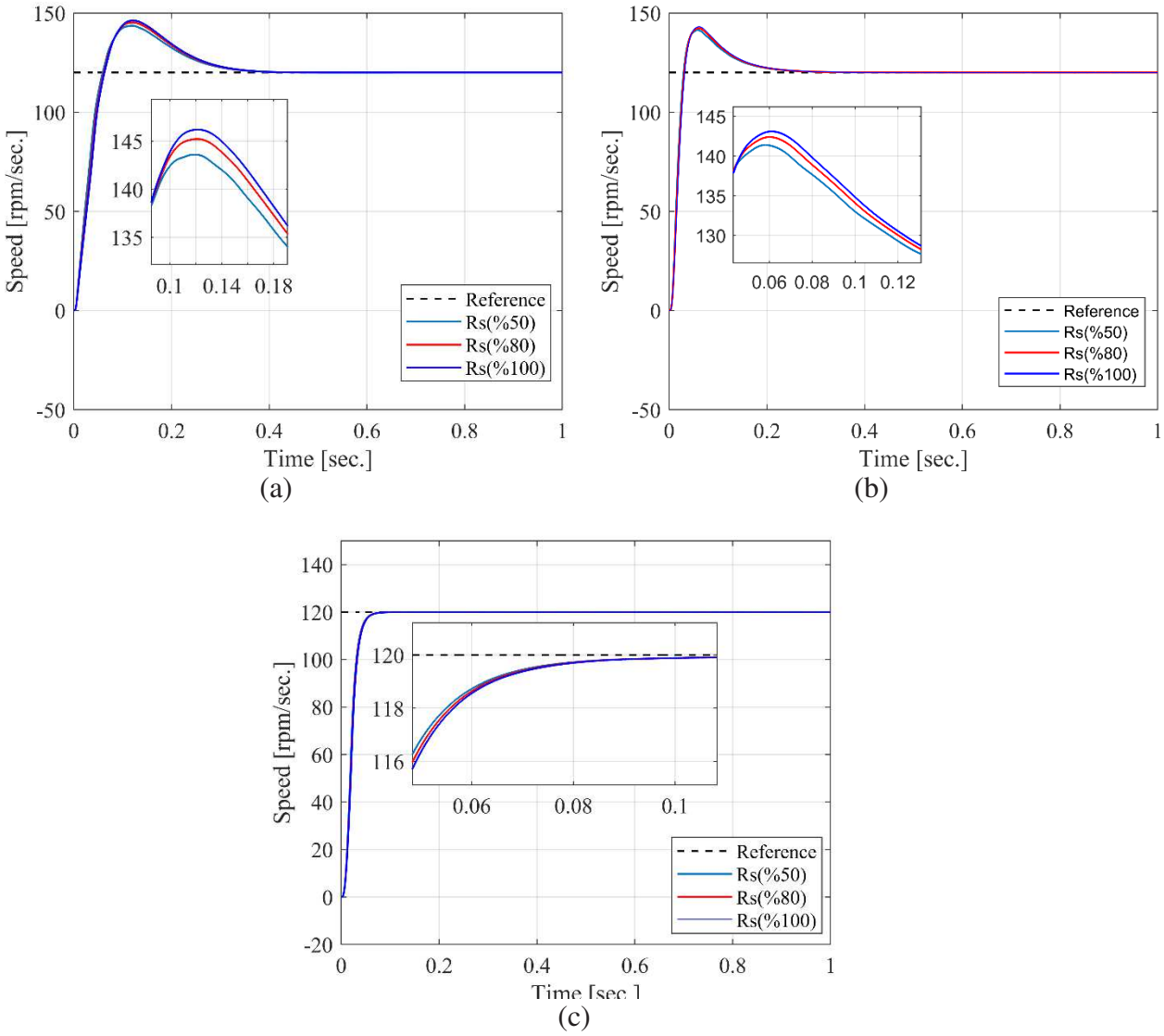

Figure 10. Speed responses variation of Rs parameter a) Conventional PI control b) SM control, c) FOSM control

In Figure 10, the response of the motor to the stator resistance changes is examined. As can be seen, the proposed FOSMC structure shows the best response at 50-80% and 100% increase in resistance change. While the durations such as overshoot and settling time increased in other control structures, the proposed control structure was almost unaffected.

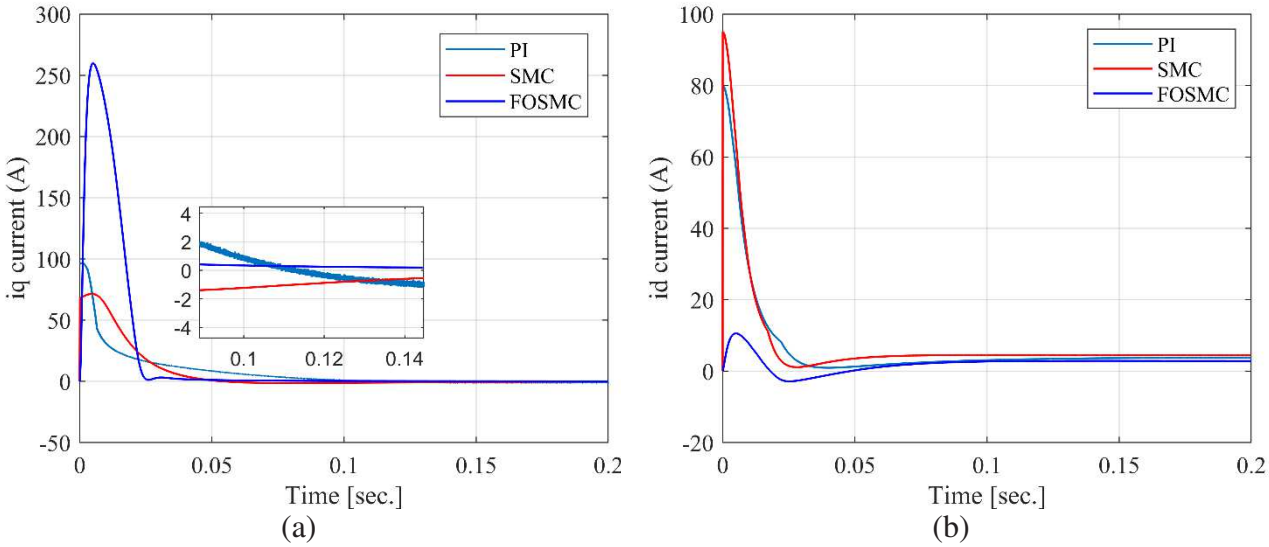

Figure 11. id and iq currents

In Figure 11, graphs of d-q axis currents are given. In (a), the current q gives the best response as overshoot at no-load in the SMC structure, while the proposed FOSMC structure responds better in terms of settling time and chattering effect. In (b), the current d has achieved the best overshoot and settling time with the proposed structure when the motor is at no load.

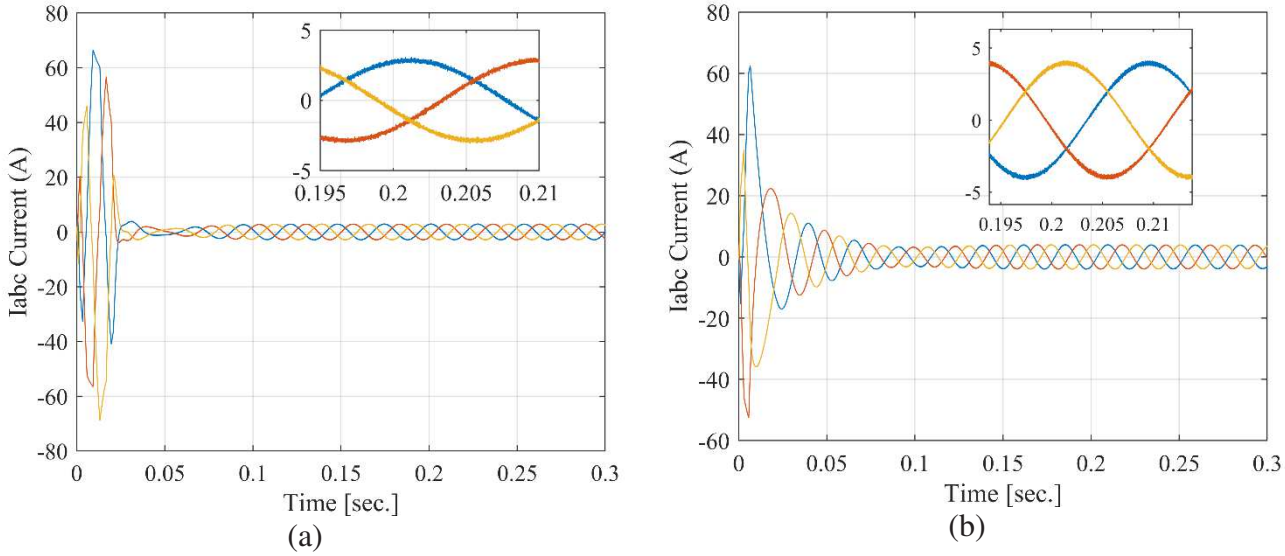

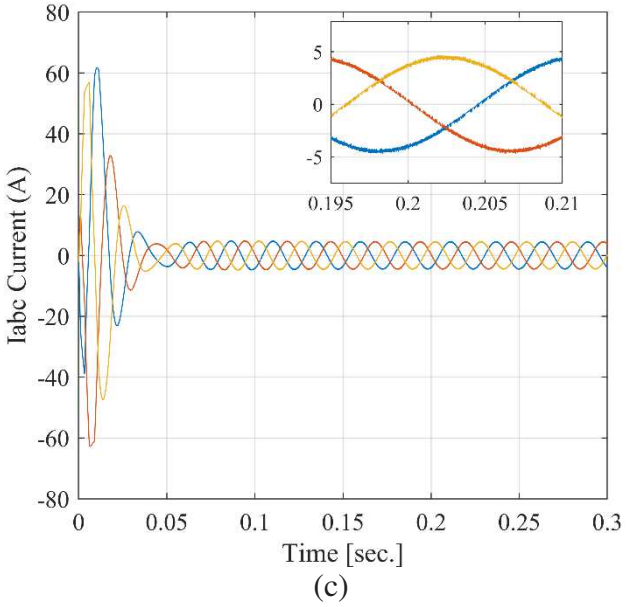

Figure 12. Iabc stator currents a) Conventional PI control, b) SM control, c) FOSM control

Three-phase stator current graphs of the motor are shown in Figure 12. As can be seen from these graphs, the reduction of the chattering effect planned to be obtained with the proposed structure has been achieved to a great extent.

CONCLUSION

In this study, the PI method, which is the FO controller of an IM, is analyzed and compared for various situations using the Matlab/Simulink program under the same conditions and the same initial conditions as the classical SMC and FOSMC methods. From the simulation results, it is seen that the FOSMC method is superior to PI and SMC for the control of IM. According to the graphics, the system controlled by FOSMC has less overshoot and it can be seen that it reaches the desired reference speed more quickly under load with less setting time. In addition, it is determined that the FOSMC method shows a more robust behavior against distorting effects such as parameter changes.

In the light of the data obtained from the study, clear results have been revealed about both the applications and designs of the FOSMC unit. According to these results, FOSMC has provided a more effective performance in the control of systems than PI and SMC, thanks to the flexibility provided by the fractional integral and derivative terms in its structures. In terms of operating conditions, it has been shown in this study that non-linear IM speed control gives better results in practice by using FOSMC instead of SMC or PI. In future work, the proposed controller can be further improved by including an artificial intelligence tuning mechanism to optimize the parameters of the controller to improve its performance. In addition, the fractional-order values used in the controller can be designed to be adaptive depending on the machine dynamics and external factors. Apart from that, the proposed controller can be extended with suitable estimators to realize sensorless control of electrical machines.

Declarations

Data Availability Statement The datasets generated during and/or analyzed during the current study are available from the corresponding author on reasonable request.

Conflict of interest The authors declare that they have no conflict of interest.

REFERENCES

[1] Quang, Nguyen Phung, and Jörg-Andreas Dittrich. *Vector control of three-phase AC machines*. Vol. 2. Heidelberg: springer, 2008.

[2] B. M. Wilamowski and J. D. Irwin, Second Edition: The Industrial Electronics Handbook -Power Electronics and Motor Drives, CRC Press, 2011.

[3] Santisteban, José Andrés, and Richard M. Stephan. "Vector control methods for induction machines: an overview." *IEEE Transactions on Education* 44.2 (2001): 170-175.

[4] Wang, Fengxiang, et al. "Advanced control strategies of induction machine: Field oriented control, direct torque control and model predictive control." *Energies* 11.1 (2018): 120.

[5] Oliveira, Carlos MR, et al. "Vector control of induction motor using an integral sliding mode controller with anti-windup." *Journal of Control, Automation and Electrical Systems* 27.2 (2016): 169-178.

[6] Talla, Jakub, et al. "Adaptive speed control of induction motor drive with inaccurate model." *IEEE Transactions on Industrial Electronics* 65.11 (2018): 8532-8542.

[7] Li, Linjie, et al. "Adaptive Damping Variable Sliding Mode Control for an Electrohydrostatic Actuator." *Actuators*. Vol. 10. No. 4. Multidisciplinary Digital Publishing Institute, 2021.

[8] Ferdiansyah, Indra, Era Purwanto, and Novie Ayub Windarko. "Fuzzy gain scheduling of PID (FGS-PID) for speed control three phase induction motor based on indirect field oriented control (IFOC)." *EMITTER International Journal of Engineering Technology* 4.2 (2016): 237-258.

[9] Fauzi, Rizana, Dedid Cahya Happyanto, and Indra Adji Sulistijono. "Fast Response Three Phase Induction Motor Using Indirect Field Oriented Control (IFOC) Based On Fuzzy-Backstepping." *EMITTER International Journal of Engineering Technology* 3.1 (2015): 92-114.

[10] Ouali, Mohamed, and Mohamed BA Kamoun. "Field-oriented control induction machine and control by sliding mode." *Simulation Practice and theory* 5.2 (1997): 121-136.

[11] Barambones, O., A. J. Garrido, and F. J. Maseda. "Integral sliding-mode controller for induction motor based on field-oriented control theory." *IET Control Theory & Applications* 1.3 (2007): 786-794.

[12] Cheng, Xin, Huashan Liu, and Wenke Lu. "Chattering-suppressed sliding mode control for flexible-joint robot manipulators." *Actuators*. Vol. 10. No. 11. Multidisciplinary Digital Publishing Institute, 2021.

[13] Kikuuwe, Ryo, Pablo J. Prieto, and Jorge-Antonio López-Rentería. "Chattering of proxy-based sliding mode control in the presence of parasitic dynamics." *IMA Journal of Mathematical Control and Information* 38.1 (2021): 177-191.

[14] Lu, Yingtao, et al. "Improved Sliding Mode-Active Disturbance Rejection Control of Electromagnetic Linear Actuator for Direct-Drive System." *Actuators*. Vol. 10. No. 7. Multidisciplinary Digital Publishing Institute, 2021.

[15] Du, Chenglong, et al. "A novel asynchronous control for artificial delayed Markovian jump systems via output feedback sliding mode approach." *IEEE Transactions on Systems, Man, and Cybernetics: Systems* 49.2 (2018): 364-374.

[16] Brandtstädter, Heide. *Sliding mode control of electromechanical systems*. Diss. Technische Universität München, 2009.

[17] Kumar, Jitendra, Vineet Kumar, and K. P. S. Rana. "Design of robust fractional order fuzzy sliding mode PID controller for two link robotic manipulator system." *Journal of Intelligent & Fuzzy Systems* 35.5 (2018): 5301-5315.

[18] Ullah, Nasim, Songshan Han, and M. I. Khattak. "Adaptive fuzzy fractional-order sliding mode controller for a class of dynamical systems with uncertainty." *Transactions of the Institute of Measurement and Control* 38.4 (2016): 402-413.

[19] Ravandi, Abbas Karamali, Esmaeel Khanmirza, and Kamran Daneshjou. "Hybrid force/position control of robotic arms manipulating in uncertain environments based on adaptive fuzzy sliding mode control." *Applied Soft Computing* 70 (2018): 864-874.

[20] Saghafinia, Ali, et al. "Adaptive fuzzy sliding-mode control into chattering-free IM drive." *IEEE Transactions on Industry Applications* 51.1 (2014): 692-701.

[21] Ho, H. F., Yiu-Kwong Wong, and Ahmad B. Rad. "Adaptive fuzzy sliding mode control with chattering elimination for nonlinear SISO systems." *Simulation Modelling Practice and Theory* 17.7 (2009): 1199-1210.

[22] Roopaei, Mehdi, and M. Zolghadri Jahromi. "Chattering-free fuzzy sliding mode control in MIMO uncertain systems." *Nonlinear Analysis: Theory, Methods & Applications* 71.10 (2009): 4430-4437.

[23] Yau, Her-Terng, and Chieh-Li Chen. "Chattering-free fuzzy sliding-mode control strategy for uncertain chaotic systems." *Chaos, Solitons & Fractals* 30.3 (2006): 709-718.

[24] Wai, Rong-Jong. "Fuzzy sliding-mode control using adaptive tuning technique." *IEEE Transactions on Industrial Electronics* 54.1 (2007): 586-594.

[25] Efe, Mehmet Önder, and Cosku Kasnakoğlu. "A fractional adaptation law for sliding mode control." *International Journal of Adaptive Control and Signal Processing* 22.10 (2008): 968-986.

[26] Muñoz-Vázquez, Aldo-Jonathan, Vicente Parra-Vega, and A. Sánchez-Orta. "Continuous fractional sliding mode-like control for exact rejection of non-differentiable Hölder disturbances." *IMA Journal of Mathematical Control and Information* 34.2 (2017): 597-610.

[27] Ullah, Nasim, et al. "Fractional order adaptive fuzzy sliding mode controller for a position servo system subjected to aerodynamic loading and nonlinearities." *Aerospace Science and Technology* 43 (2015): 381-387.

[28] Ren, Hai-Peng, et al. "Fractional order sliding mode control of a pneumatic position servo system." *Journal of the Franklin Institute* 356.12 (2019): 6160-6174.

[29] Bouakkaz, Mohammed Salah, et al. "Dynamic performance evaluation and improvement of PV energy generation systems using Moth Flame Optimization with combined fractional order PID and sliding mode controller." *Solar Energy* 199 (2020): 411-424.

[30] AKINAL, G, Sliding Mode Control and Its Applications, Gaziantep Üniversitesi, Ph.D. Thesis in Electrical and Electronic Engineering, July 2005

[31] Perruquetti, Wilfrid, and Jean Pierre Barbot, eds. *Sliding mode control in engineering*. Vol. 11. New York: Marcel Dekker, 2002.

[32] UTKIN, V., GULDNER, J., SHI, J., Sliding Mode Control in Electromechanical Systems, Taylor&Francis Inc., 325 Chestnut Street, Philadelphia, PA 19106,1999

[33] Mukhopadhyay, Shayok. *Fractional order modeling and control: development of analog strategies for plasma position control of the STOR-1M tokamak*. Utah State University, 2009.

[34] Caputo, Michele. "Linear models of dissipation whose Q is almost frequency independent—II." *Geophysical Journal International* 13.5 (1967): 529-539.

[35] Miller, Kenneth S., and Bertram Ross. *An introduction to the fractional calculus and fractional differential equations*. Wiley, 1993.

[36] Podlubny, Igor. "Fractional-order systems and PI/sup/spl lambda//D/sup/spl mu//-controllers." *IEEE Transactions on automatic control* 44.1 (1999): 208-214.

[37] Matignon, Denis. "Stability properties for generalized fractional differential systems." *ESAIM: proceedings*. Vol. 5. EDP Sciences, 1998.